

M³ashy: Multi-Modal Material Synthesis via Hyperdiffusion

Chenliang Zhou, Zheyuan Hu, Alejandro Sztrajman, Yancheng Cai, Yaru Liu, Cengiz Oztireli

Department of Computer Science and Technology, University of Cambridge
chenliang.zhou@cst.cam.ac.uk

Abstract

High-quality material synthesis is essential for replicating complex surface properties to create realistic scenes. Despite advances in the generation of material appearance based on analytic models, the synthesis of real-world measured BRDFs remains largely unexplored. To address this challenge, we propose M³ashy, a novel **multi-modal material synthesis** framework based on **hyperdiffusion**. M³ashy enables high-quality reconstruction of complex real-world materials by leveraging neural fields as a compact continuous representation of BRDFs. Furthermore, our multi-modal conditional hyperdiffusion model allows for flexible material synthesis conditioned on material type, natural language descriptions, or reference images, providing greater user control over material generation. To support future research, we contribute two new material datasets and introduce two BRDF distributional metrics for more rigorous evaluation. We demonstrate the effectiveness of M³ashy through extensive experiments, including a novel statistics-based constrained synthesis, which enables the generation of materials of desired categories.

1 Introduction

Material synthesis plays a crucial role in visual computing, enabling the creation of realistic material appearances for applications in scene understanding (Gupta, Arbelaez, and Malik 2013), material recognition (Bell et al. 2015), intrinsic image decomposition (Bousseau, Paris, and Durand 2009), generative image synthesis (Karras, Laine, and Aila 2019), and physics-based vision for simulation (Wu et al. 2017). Material appearance is commonly modeled by the *bidirectional reflectance distribution function (BRDF)*. Although there has been significant progress (e.g., Gatys, Ecker, and Bethge 2015; Zhou et al. 2018) in generative modeling of analytic BRDFs (Phong 1975; Walter et al. 2007), there is a lack of work focusing on that of measured ones. For the analytic BRDFs, the actual per-point reflectance model is typically relatively simple and low-dimensional (Ngan, Durand, and Matusik 2005; Guarnera et al. 2016). In contrast, a measured BRDF is tabulated from real-world capture and can be substantially higher-dimensional (e.g., Matusik et al. 2003), with the ability to represent complex and irregular

scattering behaviors that exceed the expressiveness of analytic models (Ngan, Durand, and Matusik 2005). However, the high-dimensionality often hinders the performance of learning-based methods. To address this gap, we propose M³ashy, a framework for realistic material generation that leverages neural fields (Sztrajman et al. 2021) as an alternative low-dimensional continuous representation for material appearance that combines high-quality reconstruction with memory efficiency. This simplifies the learning process, enabling the model to capture the underlying material distribution more efficiently.

An additional challenge in material synthesis is the lack of robust quantitative metrics for evaluating synthesis quality, making it difficult to assess and compare different approaches, unlike generative models in other fields (Theis, van den Oord, and Bethge 2016; Betzalel et al. 2022). A final limitation is the absence of multi-modal conditioning, which would enable users to guide the synthesis process using diverse inputs, such as material type, text descriptions or reference images. This limitation reduces the flexibility and control available to artists and designers. To address these limitations, we propose a set of novel BRDF distributional metrics and leverage a multi-modal conditional hyperdiffusion model to support flexible user input.

The main contributions of this work are as follows:

- A novel material synthesis pipeline using a multi-modal conditional hyperdiffusion model that supports user-specified material generation via material type, natural language descriptions, or image references.
- A thorough evaluation of M³ashy’s effectiveness, including a set of novel BRDF distributional metrics and a novel constrained synthesis experiment to synthesize materials of desired categories.
- Two new datasets: AugMERL, an enhanced collection of tabulated BRDF values, and NeuMERL, a dataset of materials represented through INRs.

2 Related Work

Material modeling Material appearance has been widely modeled by the *bidirectional reflectance distribution function (BRDF)* (Nicodemus et al. 1977; Guarnera et al. 2016; Montes and Ureña 2012; Ngan, Durand, and Matusik 2005; Westin, Li, and Torrance 2004). While analytic BRDF models (Phong 1975; Cook and Torrance 1982; Walter et al.

BRDF modeling method	Measured	Generative	Type	Text	Image	CS	Datasets	Metrics
DeepBRDF (Hu et al. 2020)	✓	✗	✗	✗	✓	✗	✗	✗
Henzler et al. (2021)	✗	✓	✗	✗	✓	✗	✗	✓
MATLABER (Xu et al. 2023)	✗	✓	✗	✓	✗	✗	✗	✗
Memery, Cedron, and Subr (2023)	✗	✓	✗	✓	✗	✗	✗	✗
Gokbudak et al. (2023)	✓	✗	✗	✗	✓	✗	✗	✗
M ³ ashy (ours)	✓	✓	✓	✓	✓	✓	✓	✓

Table 1: Comparison of material modeling methods. Our M³ashy is the first generative pipeline for measured real-world materials that supports both unconditional and multi-modal conditional synthesis guided by type, text, or image. It also enables a statistics-based constrained synthesis (CS) and introduces novel datasets and material distributional metrics.

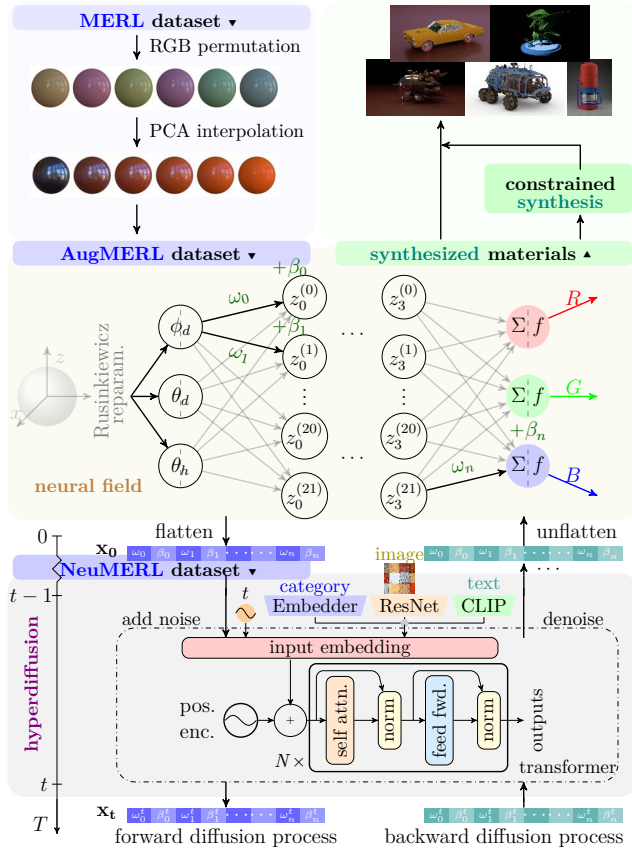


Figure 2: An overview of M³ashy, our novel neural material synthesis framework, consisting of three main stages. 1 (top left): Data augmentation using RGB permutation and PCA interpolation to create an expanded dataset, *AugMERL*; 2 (middle): Neural field fitted to individual materials, resulting in *NeuMERL*, a dataset of neural material representations; and 3 (bottom): Training a multi-modal conditional hyperdiffusion on *NeuMERL* to enable conditional synthesis of high-quality, diverse materials guided by inputs such as material type, text descriptions, or reference images. We further propose a novel statistics-based constrained synthesis method to generate materials of a specified type (top right).

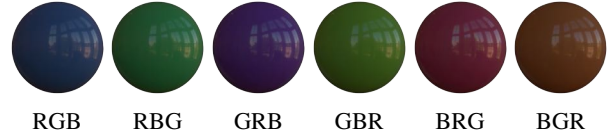


Figure 3: Six RGB permutations of the MERL material *blue acrylic*. (a) represents the original material. This permutation strategy expands the dataset by a factor of 6.

reduce the dimensionality of the BRDF data from D_{MERL} to 300. In this lower-dimensional space, we perform linear interpolation to further augment the dataset, expanding it to 2400 materials. Compared to direct linear interpolation in the high-dimensional BRDF space, interpolation in PCA space is more effective in capturing the underlying structure of the BRDF data and yields perceptually accurate results (Matusik et al. 2003; Lawrence, Rusinkiewicz, and Ramamoorthi 2004; Romeiro and Zickler 2010). An example of materials generated through PCA interpolation is shown in Fig. 4. We refer to this augmented dataset as *Augmented MERL (AugMERL)*. For additional details on PCA, please see Sec. B.1 in the supplementary.

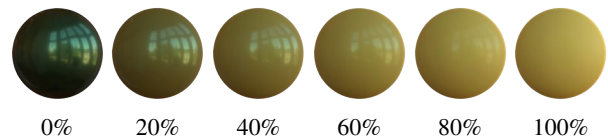


Figure 4: Linear interpolation of two MERL materials, (a) *green metallic paint* and (f) *yellow plastic*, in the PCA space.

3.2 Neural Field Fitting

Neural fields provide a low-dimensional, continuous representation for material data. Following prior work (Sztrajman et al. 2021), we overfit a compact neural field f_r^ξ parameterized by ξ , to each material in *AugMERL*. Once fitted, we treat the flattened weights of f_r^ξ as the material’s neural representation. With 2400 materials in *AugMERL*, this process yields a dataset of 2400 neural material representations, which we refer to as *Neural MERL (NeuMERL)*.

Representing materials as flattened 1D vectors enables a flexible framework for modeling complex distributions, ab-

strating away the underlying data’s dimensionality. This approach makes our pipeline adaptable to diverse data formats. In the following section, we detail three key techniques employed in fitting the neural fields.

Rusinkiewicz reparametrization In our preliminary experiments and other studies (e.g., Sztrajman et al. 2021; Zhou et al. 2024), it is observed that directly using the conventional BRDF input format – namely the incident and outgoing directions $\omega_i, \omega_o \in \mathbb{R}^3$ – can complicate the fitting process for certain materials and occasionally introduce undesirable artifacts possibly due to the high dimensionality of the input. To address this, we employ the Rusinkiewicz reparametrization (Rusinkiewicz 1998), which defines the half and difference vectors \mathbf{h} and \mathbf{d} as follows:

$$\mathbf{h} := \frac{\omega_i + \omega_o}{\|\omega_i + \omega_o\|}; \quad \mathbf{d} := R_{\hat{\mathbf{b}}, -\theta_h} R_{\hat{\mathbf{n}}, -\varphi_h} \omega_i, \quad (1)$$

where $R_{\mathbf{v}, \alpha}$ denotes a rotation around the vector \mathbf{v} by the angle α , $\hat{\mathbf{n}}$ is the surface normal, and $\hat{\mathbf{b}}$ is the surface binormal. This reparametrization helps improve the robustness of the neural field fitting process by addressing reciprocity constraints more directly (Sztrajman et al. 2021; Zhou et al. 2024).

We then proceed by adopting the spherical coordinates of the half and difference vectors \mathbf{h} and \mathbf{d} , specifically $\theta_h, \varphi_h, \theta_d, \varphi_d$, as inputs to our neural fields. A further advantage of using the Rusinkiewicz reparametrization is that, since our materials are isotropic, the BRDF remains invariant with respect to φ_h . Consequently, we can omit this parameter, reducing the input complexity from $(\omega_i, \omega_o) \in \mathbb{R}^6$ to $(\theta_h, \theta_d, \varphi_d) \in [0, \frac{\pi}{2}]^2 \times [0, \pi)$. This reparametrization enhances the efficiency of our neural field representation without sacrificing accuracy.

Mean absolute logarithmic loss The high dynamic range of BRDF values makes fitting reflectance data particularly sensitive to error distribution. For low reflectance values, even minor fitting errors can have a large impact on the loss, causing shifts in perceived “hue” in rendered images, which leads to unrealistic colors and reduced visual fidelity. To address these issues, we employ a mean absolute logarithmic loss for BRDF values (Sztrajman et al. 2021):

$$\mathcal{L}_{\text{NF}}(\boldsymbol{\xi}) := \mathbb{E}_{\theta_h, \theta_d, \varphi_d} \left[\left| \log(1 + f_r \cos \theta_i) - \log(1 + f_r^\xi \cos \theta_i) \right| \right] \quad (2)$$

where f_r denotes the ground-truth BRDF, and θ_i is the polar angle of the incident direction. This loss is computed per color channel, offering a balanced approach that stabilizes training across samples with both low and high values. Consequently, it enhances the model’s capability to manage dynamic reflectance variations, leading to more realistic color reproduction and improved visual fidelity.

Weight initialization Ideally, the neural materials in NeuMERL should originate from a consistent distribution. However, due to a phenomenon known as *weight symmetry* (Liao, Leibo, and Poggio 2016), we observe that different

weights can yield the same neural field. For instance, swapping weights between two neurons in a hidden layer, or flipping the signs of both input and output weights for a neuron before an odd, linear, or piecewise-linear activation function like ReLU (Nair and Hinton 2010), results in an identical neural field. To address this, we propose using the optimized weights from the first fitted neural field as the initialization for subsequent neural field fittings. This approach helps align the weights across all fitted fields, promoting consistency within NeuMERL and facilitating smoother training of the hyperdiffusion model in the next stage.

3.3 Multi-Modal Conditional Hyperdiffusion

To model the complex distribution within the NeuMERL dataset, we utilize a diffusion process (Ho, Jain, and Abbeel 2020; Peebles et al. 2022; Erkoç et al. 2023). Specifically, we employ a transformer-based denoising network (Vaswani 2017), leveraging its demonstrated efficacy (Peebles et al. 2022) and its attention mechanisms allowing for an effective focus on relevant information, enhancing the network’s ability to capture intricate dependencies in the data.

Our hyperdiffusion supports conditioning across three modalities: material type (represented as integers), text description, and reference images. We utilize a categorical encoding for material type, an augmented CLIP text embedding (Radford et al. 2021; Zhou, Zhong, and Oztireli 2023) for text, and a ResNet (He et al. 2016) for images. This multi-modal conditioning approach enables material synthesis to be guided by different user inputs, enhancing workflow intuitiveness and accessibility and allowing for a more smooth and accurate translation of creative vision into generated materials. For conditional sampling, we employ classifier-free guidance (CFG) (Ho and Salimans 2022).

Please refer to Secs. B.2, B.3, C.2 and D.2 in the supplementary for further details on the diffusion model, transformer, attention mechanism, and CFG, respectively.

4 Experiments

In this section, we present extensive experiments on M³ashy. For additional details, please refer to the appendix: model and experiment specifics in Secs. C and D, further results in Sec. F, and more experiments in Sec. G.

4.1 Dataset

We fit neural fields to individual materials in the AugMERL dataset (Sec. 3.1), which is derived from the MERL BRDF dataset (Matusik et al. 2003). Our hyperdiffusion model is trained on the NeuMERL dataset (Sec. 3.2), which consists of neural material representations. The training-validation split is 80%-20% for each individual fitting on AugMERL and 95%-5% for NeuMERL. All samples derived from a given material remain within one split. In the constrained synthesis experiments in Sec. 4.5, statistical information is gathered from the MERL dataset (Matusik et al. 2003).

4.2 Material Distributional Metrics

We use Fréchet Inception Distance (FID) (Heusel et al. 2017) as an image-based metric to assess the quality of rendered single-view images.

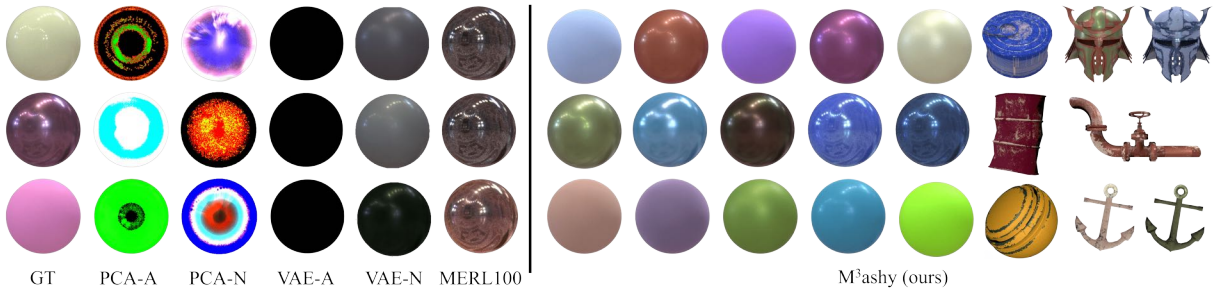


Figure 5: Material synthesis. Baseline models fail to capture the underlying distribution effectively, resulting in homogeneous outputs or severe artifacts. In contrast, M³ashy successfully captures the complex neural material distribution, achieving significantly better fidelity and diversity. Our materials also support spatially varying rendering configurations (last three columns).

To the best of our knowledge, effective metrics directly comparing material distributions are still lacking. Drawing inspiration from the metrics for point clouds (Yang et al. 2019), we introduce three novel material distributional metrics – minimum matching distance (MMD), coverage (COV), and 1-nearest neighbor (1-NNA) – to evaluate the fidelity and diversity of synthesized BRDF sets \mathcal{S} relative to a reference set \mathcal{R} . Each metric is based on an underlying distance measure $d(f_r, f'_r)$ between two BRDFs.

Minimum matching distance (MMD) MMD measures the average distance from each reference BRDF to its nearest synthesized counterpart:

$$\mathcal{L}_{\text{MMD}}^d(\mathcal{R}, \mathcal{S}) := \frac{1}{|\mathcal{R}|} \sum_{f_r \in \mathcal{R}} \min_{f'_r \in \mathcal{S}} d(f_r, f'_r) \quad (3)$$

MMD evaluates the fidelity of the synthesized set relative to the reference, with a lower score indicating higher fidelity.

Coverage (COV) COV calculates the proportion of reference BRDFs that are “covered” by the synthesized set. A reference BRDF is considered covered if it is the closest neighbor to at least one synthesized BRDF:

$$\mathcal{L}_{\text{COV}}^d(\mathcal{R}, \mathcal{S}) = \frac{\left| \left\{ \underset{f'_r \in \mathcal{S}}{\operatorname{argmin}} d(f_r, f'_r) \mid f_r \in \mathcal{R} \right\} \right|}{|\mathcal{R}|} \quad (4)$$

COV assesses the diversity of the synthesized set, with a higher score reflecting better coverage.

1-nearest neighbor (1-NNA) 1-NNA is a leave-one-out metric that measures the similarity between the reference and synthesized BRDF distributions, capturing both diversity and fidelity:

$$\mathcal{L}_{\text{1-NNA}}^d(\mathcal{R}, \mathcal{S}) := \frac{\sum_{f_r \in \mathcal{R}} \mathbb{I}[N_{f_r} \in \mathcal{R}] + \sum_{f'_r \in \mathcal{S}} \mathbb{I}[N_{f'_r} \in \mathcal{S}]}{|\mathcal{S}| + |\mathcal{R}|}, \quad (5)$$

where $\mathbb{I}[\cdot]$ is the indicator function and N_{f_r} denotes the nearest neighbor of f_r in $(\mathcal{R} \cup \mathcal{S}) - \{f_r\}$. In this metric, each sample is classified as belonging to either the reference set \mathcal{R} or the synthesized set \mathcal{S} based on the membership of its nearest neighbor. If \mathcal{R} and \mathcal{S} are drawn from the same underlying distribution, the classifier’s accuracy will approach 50% with a large sample size.

Each metric can be computed using an underlying distance d . Potential options include rendering-based metrics such as root mean squared error (RMSE), peak signal-to-noise ratio (PSNR), and structural similarity index measure (SSIM) (Wang et al. 2004). Since higher values in PSNR and SSIM correspond to greater similarity, we negate these values – resulting in NegPSNR and NegSSIM, respectively – to make them plausible distance functions. To directly assess the distance between two BRDFs without relying on renderings, we also introduce the following BRDF L1 distance:

$$d_{\text{BRDF-L1}} := \mathbb{E}_{\theta_h, \theta_d, \varphi_d} [|f_r - f'_r|]; \quad (6)$$

For further background on the image-based metrics and validation of the proposed material distributional metrics, please refer to Sec. E in the supplementary.

4.3 Unconditional Synthesis

We begin by presenting the results of unconditional synthesis of neural materials using M³ashy. We compare our approach with the PCA-based method of Nielsen, Jensen, and Ramamoorthi (2015) and with the sparse reconstruction model of Gokbudak et al. (2023), which uses a hypernetwork to model measured tabular BRDF data. As Gokbudak et al.’s method is not generative, we extend it with a variational autoencoder (VAE) to enable comparison. Both methods are applied to the AugMERL (-A) and NeuMERL (-N) datasets, resulting in four baselines: VAE-A, VAE-N, PCA-A, and PCA-N. We also develop another baseline, MERL100, that represents our method trained on the original MERL dataset to demonstrate the effectiveness of our data augmentation.

Table 2 provides a detailed comparison of baselines with our proposed metrics, while Figs. 1 and 5 showcase renderings of these materials across various geometries and scenes. To achieve more complex visual effects, our synthesized materials support rendering with bump or normal maps, as well as spatially varying configurations (Jakob et al. 2022) (additional results in Sec. F). The quantitative and qualitative results indicate that M³ashy consistently outperforms all baselines across metrics, producing diverse, high-quality, visually appealing, and perceptually realistic renderings. This demonstrates the effectiveness of M³ashy for neural material

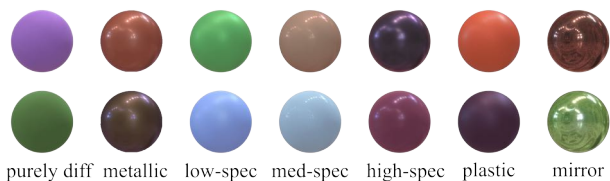


Figure 6: Synthesized materials of seven distinct categories using our novel constrained synthesis. Grounded in BRDF statistical analysis, this approach provides enhanced explainability and interpretability compared to standard conditional synthesis methods.

synthesis. Notably, materials synthesized by some baselines exhibit significant artifacts, likely due to the limitations of these simpler models in capturing the complex distribution of measured materials.

4.4 Multi-Modal Conditional Synthesis

To further evaluate the effectiveness of our pipeline, we perform multi-modal conditional synthesis by conditioning our model on various modalities of input: material type, text description, or material images.

For material type conditioning, we represent each of the 48 material types in the MERL dataset (Matusik et al. 2003) (e.g., *acrylic*, *metallic*, *plastic*, etc.) using integers. The full list of material types is available in Sec. D.3 in the supplementary; For text conditioning, we use descriptions derived from the MERL dataset (Matusik et al. 2003). For additional materials in the AugMERL dataset, descriptions are assigned as follows: For RGB-permuted materials, we retain the original description but omit color-specific words (e.g., “*red metallic paint*” becomes “*metallic paint*”); For PCA-interpolated materials, we generate descriptions in the format “*a mixture of t_A and t_B* ”, where t_A and t_B are the descriptions of the interpolated materials A and B , respectively; For image-based conditioning, we use cropped single-view renderings of materials from AugMERL as input. We encode input texts and images using CLIP encoders (Radford et al. 2021).

Figures 7 to 9 present the results for type-, text-, and image-conditioned synthesis, respectively. Across all conditioning modes, the synthesized materials demonstrate realism, diversity, and a close alignment with the input conditions. Notably, in text- and image-conditioned synthesis, M³ashy effectively generalizes to unseen texts (e.g., “*green metal*”, “*red plastic*”, and “*highly specular material*”) and real-world images, producing materials that are perceptually consistent with these previously unseen inputs.

4.5 Constrained Synthesis

We classify materials into seven categories based on their reflective properties: *diffuse*, *metallic*, *low-specular*, *medium-specular*, *high-specular*, *plastic*, and *mirror*. To enable the synthesis of materials within a specified category, we introduce a novel approach called *constrained synthesis*. This statistics-based method complements our conditional

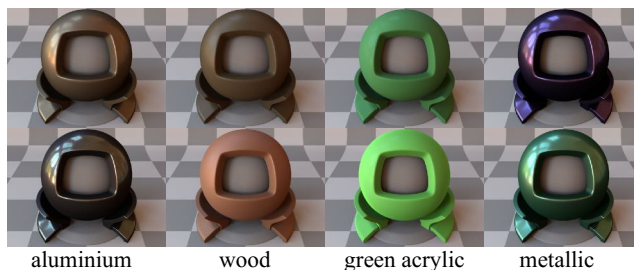


Figure 7: Type-conditioned synthesis. The synthesized materials are diverse and closely align with the input type.



Figure 8: Text-conditioned synthesis. Synthesized materials align with the texts and generalize to unseen inputs: “*green metal*”, “*red plastic*”, and “*highly specular material*”.

pipeline by enforcing constraints on unconditionally synthesized samples, allowing for targeted material generation according to desired reflective characteristics.

We derive the theoretical upper limit for a diffuse reflectance value, f_{diffuse} , for a constant (i.e., purely diffuse) BRDF $f_r(\omega_i, \omega_o) \equiv f_{\text{diffuse}}$ in each color channel. For a physically valid BRDF that adheres to energy passivity (Zhou et al. 2024), the reflected energy must not exceed the incident energy in each channel. Thus, we have:

$$1 \geq \int_{H^2} f_r(\omega_i, \omega_o) \cos \theta_o \, d\omega_o \quad (7)$$

$$= f_{\text{diffuse}} \int_{H^2} \cos \theta_o \, d\omega_o = \pi f_{\text{diffuse}} \Rightarrow f_{\text{diffuse}} \leq \frac{1}{\pi}. \quad (8)$$

Building on this observation and a statistical analysis of the MERL’s mean and maximum reflectance values across color channels and material types (Sec. G.1 in the supplementary), we propose a set of rules for categorizing materials into seven types. These rules enable the selection of synthesized materials based on desired material characteristics. Unlike many black-box machine learning approaches, this method is rooted in BRDF analysis, offering inherent

	Metric	Training set	PCA-A	PCA-N	VAE-A	VAE-N	MERL100	M ³ ashy (ours)
	FID (↓)	0.187	10.9	23.8	26.1	10.0	7.56	0.440
MMD (↓)	BRDF-L1×10 ⁻³	2.51	9.05	9.22	9.09	5.83	4.30	4.02
	RMSE×10 ²	7.54	33.3	30.2	63.7	15.5	13.4	9.34
	NegPSNR	-28.7	-13.9	-14.8	-8.30	-20.9	-22.6	-25.6
	NegSSIM×10	-9.55	-6.74	-6.29	-2.68	-6.86	-8.27	-9.40
COV (%) (↑)	BRDF-L1	60.8	2.50	30	0.833	20.8	28.3	50.8
	RMSE	55.8	18.3	28.3	0.833	16.7	25.0	50.0
	NegPSNR	56.7	18.3	28.3	0.833	18.3	25.0	50.0
	NegSSIM	59.2	23.3	16.7	0.833	17.5	22.5	51.7
1-NNA (%) (↓)	BRDF-L1	58.8	100	95.4	100	96.7	92.5	80.0
	RMSE	55.4	96.3	93.4	100	93.3	84.6	60.0
	NegPSNR	55.0	94.2	90.0	100	93.3	84.6	60.4
	NegSSIM	57.5	96.3	96.7	100	93.8	86.3	61.7

Table 2: Qualitative evaluation of unconditional synthesis with metrics assessing generation fidelity and diversity. M³ashy significantly outperforms all baseline models across these metrics, underscoring its effectiveness in neural material synthesis.



Figure 9: Image-conditioned synthesis. Each of the eight pairs consists of the input (left) and the synthesized (right). M³ashy effectively generates realistic materials that closely align with the conditioning images and generalizes to unseen, real-world images (last column).

explainability and interpretability. Below, we outline two of these rules, with the full set detailed in Sec. D.4.

- Purely diffuse materials: The reflectance values in all directions do not exceed the diffuse threshold f_{diffuse} , allowing for only $e := 8 \times 10^4$ exceptions:

$$|\{(\omega_o, \omega_i) \in \mathbb{R}^6 \mid \|f_r(\omega_o, \omega_i)\|_\infty > f_{\text{diffuse}}\}| < e, \quad (9)$$

where $\|\cdot\|_\infty$ denotes the maximum reflectance value among the three color channels.

- Metallic materials: The reflectance values in all directions exceed the diffuse threshold f_{diffuse} :

$$\forall(\omega_o, \omega_i) \in \mathbb{R}^6, \|f_r(\omega_o, \omega_i)\|_\infty > f_{\text{diffuse}} \quad (10)$$

Figure 6 shows materials generated through our constrained synthesis, incorporating the proposed filtering rules to ensure that the synthesized outputs match the specified material categories. The results demonstrate that the synthesized materials effectively exhibit the characteristics of the desired categories.

4.6 Ablation Study

To assess the impact of our augmented material dataset AugMERL, we further train our model on the original MERL dataset in the unconditional synthesis task. We report both quantitative and qualitative results for this model, presented

Metric	Sparse reconstruction		Compression	
	MERL	AugMERL	MERL	AugMERL
PSNR (↑)	32.2	36.3	45.2	48.3
Delta E (↓)	2.1	1.8	0.693	0.623
SSIM (↑)	0.972	0.983	0.994	0.994

Table 3: Quantitative comparison of training on MERL versus AugMERL in the sparse BRDF reconstruction and BRDF compression experiments. The results demonstrate that training on AugMERL consistently enhances performance across all metrics.

in the ‘‘MERL100’’ columns of Tab. 2 and Fig. 5, respectively. The results indicate that the model trained on AugMERL exhibits higher quality and diversity compared to the one trained on MERL, demonstrating the effectiveness of our augmented dataset in enhancing the synthesis pipeline.

Additionally, we conduct sparse BRDF reconstruction and BRDF compression experiments following a previous method (Gokbudak et al. 2023). For sparse reconstruction, we set the sample size to $N = 4000$, while for compression, we use a latent dimension of 40. In both experiments, we train the model on either the original MERL dataset or the AugMERL dataset. The results, summarized in Tab. 3, demonstrate that training on AugMERL consistently enhances material quality across all evaluated metrics, further validating the effectiveness of our augmented dataset.

5 Conclusion

We introduced M³ashy, a **multi-modal material synthesis** approach with **hyperdiffusion**. Using neural fields as the core representation, we trained hyperdiffusion on their weights, demonstrating its ability to generate high-quality, diverse materials. Additionally, we contribute two material datasets and three BRDF metrics for future research.

References

- Abdi, H.; and Williams, L. J. 2010. Principal component analysis. *Wiley interdisciplinary reviews: computational statistics*, 2(4): 433–459.
- Bangay, S.; and Radloff, J. D. 2004. Kaleidoscope configurations for reflectance measurement. In *Proceedings of the 3rd International Conference on Computer Graphics, Virtual Reality, Visualization and Interaction in Africa*, AFRIGRAPH '04, 161–170. New York, NY, USA: Association for Computing Machinery. ISBN 1581138636.
- Bell, S.; Upchurch, P.; Snavely, N.; and Bala, K. 2015. Material recognition in the wild with the materials in context database. *Proceedings of the IEEE Conference on Computer Vision and Pattern Recognition (CVPR)*, 3479–3487.
- Betzalel, E.; Penso, C.; Navon, A.; and Fetaya, E. 2022. A Study on the Evaluation of Generative Models. arXiv:2206.10935.
- Bousseau, A.; Paris, S.; and Durand, F. 2009. User-assisted intrinsic images. *ACM Transactions on Graphics (TOG)*, 28(5): 1–10.
- Burley, B. 2012. Physically-Based Shading at Disney. *SIGGRAPH Comput. Graph.*
- Chen, D. Z.; Siddiqui, Y.; Lee, H.-Y.; Tulyakov, S.; and Nießner, M. 2023a. Text2Tex: Text-driven Texture Synthesis via Diffusion Models. *2023 IEEE/CVF International Conference on Computer Vision (ICCV)*, 18512–18522.
- Chen, R.; Chen, Y.; Jiao, N.; and Jia, K. 2023b. Fantasia3D: Disentangling Geometry and Appearance for High-quality Text-to-3D Content Creation. In *Proceedings of the IEEE/CVF International Conference on Computer Vision (ICCV)*, 22246–22256.
- Cook, R. L.; and Torrance, K. E. 1982. A Reflectance Model for Computer Graphics. *ACM Trans. Graph.*, 1(1): 7–24.
- Csiszár, I. 1975. I-divergence geometry of probability distributions and minimization problems. *The annals of probability*, 146–158.
- Dana, K. J.; van Ginneken, B.; Nayar, S. K.; and Koenderink, J. J. 1999. Reflectance and texture of real-world surfaces. *ACM Trans. Graph.*, 18(1): 1–34.
- Devlin, J. 2018. Bert: Pre-training of deep bidirectional transformers for language understanding. *arXiv preprint arXiv:1810.04805*.
- Dupuy, J.; and Jakob, W. 2018a. An adaptive parameterization for efficient material acquisition and rendering. *ACM Transactions on Graphics (TOG)*, 37(6): 1–14.
- Dupuy, J.; and Jakob, W. 2018b. An Adaptive Parameterization for Efficient Material Acquisition and Rendering. *Transactions on Graphics (Proceedings of SIGGRAPH Asia)*, 37(6): 274:1–274:18.
- Erkoç, Z.; Ma, F.; Shan, Q.; Nießner, M.; and Dai, A. 2023. Hyper-Diffusion: Generating Implicit Neural Fields with Weight-Space Diffusion. In *2023 IEEE/CVF International Conference on Computer Vision (ICCV)*, 14254–14264.
- Fan, J.; Wang, B.; Hašan, M.; Yang, J.; and Yan, L.-Q. 2022. Neural Layered BRDFs. In *Proceedings of SIGGRAPH 2022*.
- Filip, J.; and Vávra, R. 2014. Template-based sampling of anisotropic BRDFs. *Computer Graphics Forum*, 33(7): 91–99.
- Gatys, L.; Ecker, A. S.; and Bethge, M. 2015. Texture synthesis using convolutional neural networks. *Advances in neural information processing systems*, 28.
- Gokbudak, F.; Sztrajman, A.; Zhou, C.; Zhong, F.; Mantiuk, R.; and Oztireli, C. 2023. Hypernetworks for Generalizable BRDF Estimation. *arXiv e-prints*, arXiv–2311.
- Guarnera, D.; Guarnera, G.; Ghosh, A.; Denk, C.; and Glencross, M. 2016. BRDF Representation and Acquisition. *Computer Graphics Forum*, 35(2): 625–650.
- Guo, J.; Li, Z.; He, X.; Wang, B.; Li, W.; Guo, Y.; and Yan, L.-Q. 2023. MetaLayer: A Meta-Learned BSDF Model for Layered Materials. *ACM Trans. Graph.*, 42(6).
- Gupta, S.; Arbelaez, P.; and Malik, J. 2013. Perceptual organization and recognition of indoor scenes from RGB-D images. *Proceedings of the IEEE Conference on Computer Vision and Pattern Recognition (CVPR)*, 564–571.
- Haindl, M.; and Filip, J. 2013. *Visual texture: Accurate material appearance measurement, representation and modeling*. Springer Science & Business Media.
- He, K.; Zhang, X.; Ren, S.; and Sun, J. 2016. Deep residual learning for image recognition. In *Proceedings of the IEEE conference on computer vision and pattern recognition*, 770–778.
- Henzler, P.; Deschaintre, V.; Mitra, N. J.; and Ritschel, T. 2021. Generative modelling of BRDF textures from flash images. *ACM Trans. Graph.*, 40(6).
- Heusel, M.; Ramsauer, H.; Unterthiner, T.; Nessler, B.; and Hochreiter, S. 2017. Gans trained by a two time-scale update rule converge to a local nash equilibrium. *Advances in neural information processing systems*, 30.
- Ho, J.; Jain, A.; and Abbeel, P. 2020. Denoising Diffusion Probabilistic Models. arXiv:2006.11239.
- Ho, J.; and Salimans, T. 2022. Classifier-Free Diffusion Guidance. arXiv:2207.12598.
- Hu, B.; Guo, J.; Chen, Y.; Li, M.; and Guo, Y. 2020. DeepBRDF: A Deep Representation for Manipulating Measured BRDF. *Computer Graphics Forum*, 39(2): 157–166.
- Hu, Y.; Guerrero, P.; Hasan, M.; Rushmeier, H.; and Deschaintre, V. 2023. Generating Procedural Materials from Text or Image Prompts. In *ACM SIGGRAPH 2023 Conference Proceedings*, 1–11.
- Jakob, W.; Speierer, S.; Roussel, N.; and Vicini, D. 2022. Dr.Jit: A Just-In-Time Compiler for Differentiable Rendering. *Transactions on Graphics (Proceedings of SIGGRAPH)*, 41(4).
- Karras, T.; Laine, S.; and Aila, T. 2019. A style-based generator architecture for generative adversarial networks. *Proceedings of the IEEE Conference on Computer Vision and Pattern Recognition (CVPR)*, 4401–4410.
- Kingma, D. P.; and Welling, M. 2013. Auto-encoding variational bayes. *arXiv preprint arXiv:1312.6114*.
- Lawrence, J.; Rusinkiewicz, S.; and Ramamoorthi, R. 2004. Efficient BRDF importance sampling using a factored representation. *ACM Transactions on Graphics (ToG)*, 23(3): 496–505.
- Li, H.; Foo, S.-C.; Torrance, K. E.; and Westin, S. H. 2006. Automated three-axis gonioreflectometer for computer graphics applications. *Optical Engineering*, 45(4): 043605.
- Liao, Q.; Leibo, J.; and Poggio, T. 2016. How important is weight symmetry in backpropagation? *Proceedings of the AAAI Conference on Artificial Intelligence*, 30(1).
- Mann, B.; Ryder, N.; Subbiah, M.; Kaplan, J.; Dhariwal, P.; Neelakantan, A.; Shyam, P.; Sastry, G.; Askell, A.; Agarwal, S.; et al. 2020. Language models are few-shot learners. *arXiv preprint arXiv:2005.14165*, 1.
- Marschner, S. R.; Westin, S. H.; Lafortune, E. P. F.; Torrance, K. E.; and Greenberg, D. P. 1999. Image-Based BRDF Measurement Including Human Skin. In Lischinski, D.; and Larson, G. W., eds., *Eurographics Workshop on Rendering*. The Eurographics Association. ISBN 3-211-83382-X.
- Matusik, W.; Pfister, H.; Brand, M.; and McMillan, L. 2003. A Data-Driven Reflectance Model. *ACM Transactions on Graphics (TOG)*, 22(3): 759–769.

- Memery, S.; Cedron, O.; and Subr, K. 2023. Generating Parametric BRDFs from Natural Language Descriptions. *Computer Graphics Forum*.
- Montes, R.; and Ureña, C. 2012. An overview of BRDF models. *University of Grenada, Technical Report LSI-2012-001*.
- Nair, V.; and Hinton, G. E. 2010. Rectified linear units improve restricted boltzmann machines. In *Proceedings of the 27th international conference on machine learning (ICML-10)*, 807–814.
- Ngan, A.; Durand, F.; and Matusik, W. 2005. Experimental Analysis of BRDF Models. *Rendering Techniques*, 2005(16th): 2.
- Nicodemus, F. E.; Richmond, J. C.; Hsia, J. J.; Ginsberg, I. W.; Limperis, T.; Harman, S.; and Baruch, J. J. 1977. *Geometrical considerations and nomenclature for reflectance*. NATIONAL BUREAU OF STANDARDS, USA.
- Nielsen, J. B.; Jensen, H. W.; and Ramamoorthi, R. 2015. On Optimal, Minimal BRDF Sampling for Reflectance Acquisition. *ACM Transactions on Graphics (TOG)*, 34(6): 186:1–186:11.
- Peebles, W.; Radosavovic, I.; Brooks, T.; Efros, A. A.; and Malik, J. 2022. Learning to learn with generative models of neural network checkpoints. *arXiv preprint arXiv:2209.12892*.
- Phong, B. T. 1975. Illumination for computer generated pictures. *Commun. ACM*, 18(6): 311–317.
- Radford, A.; Kim, J. W.; Hallacy, C.; Ramesh, A.; Goh, G.; Agarwal, S.; Sastry, G.; Askell, A.; Mishkin, P.; Clark, J.; et al. 2021. Learning transferable visual models from natural language supervision. In *International conference on machine learning*, 8748–8763. PMLR.
- Romeiro, F.; and Zickler, T. 2010. Blind reflectometry. In *Computer Vision—ECCV 2010: 11th European Conference on Computer Vision, Heraklion, Crete, Greece, September 5–11, 2010, Proceedings, Part I 11*, 45–58. Springer.
- Rusinkiewicz, S. 1998. A New Change of Variables for Efficient BRDF Representation. In *Eurographics Workshop on Rendering*. Vienna, Austria.
- Serrano, A.; Gutierrez, D.; Myszkowski, K.; Seidel, H.-P.; and Masia, B. 2016. An Intuitive Control Space for Material Appearance. *SIGGRAPH ASIA*, 35(6): 186:1–186:12.
- Song, J.; Meng, C.; and Ermon, S. 2021. Denoising diffusion implicit models. *ICLR 2021*.
- Sun, T.; Jensen, H. W.; and Ramamoorthi, R. 2018. Connecting measured brdfs to analytic brdfs by data-driven diffuse-specular separation. *ACM Transactions on Graphics (TOG)*, 37(6): 1–15.
- Sztrajman, A.; Křivánek, J.; Wilkie, A.; and Weyrich, T. 2017. Image-based Remapping of Material Appearance. In *Proc. 5th Workshop on Material Appearance Modeling*, 5–8.
- Sztrajman, A.; Křivánek, J.; Wilkie, A.; and Weyrich, T. 2019. Image-based Remapping of Spatially-Varying Material Appearance. *Journal of Computer Graphics Techniques (JCGT)*, 8(4): 1–30.
- Sztrajman, A.; Rainer, G.; Ritschel, T.; and Weyrich, T. 2021. Neural BRDF Representation and Importance Sampling. *Computer Graphics Forum*.
- Tchapmi, L. P.; Ray, T.; Tchapmi, M.; Shen, B.; Martin-Martin, R.; and Savarese, S. 2022. Generating procedural 3D materials from images using neural networks. In *Proceedings of the 2022 4th International Conference on Image, Video and Signal Processing*, 32–40.
- Theis, L.; van den Oord, A.; and Bethge, M. 2016. A note on the evaluation of generative models. *arXiv:1511.01844*.
- Vaswani, A. 2017. Attention is all you need. *Advances in Neural Information Processing Systems*.
- Walter, B.; Marschner, S. R.; Li, H.; and Torrance, K. E. 2007. Microfacet models for refraction through rough surfaces. In *Proceedings of the 18th Eurographics Conference on Rendering Techniques, EGSR'07*, 195–206. Goslar, DEU: Eurographics Association. ISBN 9783905673524.
- Wang, Z.; Bovik, A.; Sheikh, H.; and Simoncelli, E. 2004. Image quality assessment: from error visibility to structural similarity. *IEEE Transactions on Image Processing*, 13(4): 600–612.
- Weinmann, M.; Gall, J.; and Klein, R. 2014. Material Classification Based on Training Data Synthesized Using a BTF Database. In *Computer Vision - ECCV 2014 - 13th European Conference, Zurich, Switzerland, September 6-12, 2014, Proceedings, Part III*, 156–171. Springer International Publishing.
- Weinmann, M.; and Klein, R. 2015a. Advances in geometry and reflectance acquisition (course notes). In *SIGGRAPH Asia 2015 Courses, SA '15*. New York, NY, USA: Association for Computing Machinery. ISBN 9781450339247.
- Weinmann, M.; and Klein, R. 2015b. Material recognition for efficient acquisition of geometry and reflectance. In *Computer Vision - ECCV 2014 Workshops: Zurich, Switzerland, September 6-7 and 12, 2014, Proceedings, Part III 13*, 321–333. Springer.
- Westin, S. H.; Li, H.; and Torrance, K. E. 2004. A comparison of four BRDF models. In *Eurographics Symposium on Rendering*, 1–10.
- White, D. R.; Saunders, P.; Bonsey, S. J.; van de Ven, J.; and Edgar, H. 1998. Reflectometer for measuring the bidirectional reflectance of rough surfaces. *Appl. Opt.*, 37(16): 3450–3454.
- Wu, J.; Zhang, C.; Xue, T.; Freeman, W. T.; and Tenenbaum, J. B. 2017. Marnet: 3d shape reconstruction via 2.5 d sketches. *Advances in Neural Information Processing Systems*, 30.
- Xu, X.; Lyu, Z.; Pan, X.; and Dai, B. 2023. MATLABER: Material-Aware Text-to-3D via LAtent BRDF auto-Encoder. *arXiv:2308.09278*.
- Yang, G.; Huang, X.; Hao, Z.; Liu, M.-Y.; Belongie, S.; and Hariharan, B. 2019. Pointflow: 3d point cloud generation with continuous normalizing flows. In *Proceedings of the IEEE/CVF international conference on computer vision*, 4541–4550.
- Zhang, S.; Peng, S.; Xu, T.; Yang, Y.; Chen, T.; Xue, N.; Shen, Y.; Bao, H.; Hu, R.; and Zhou, X. 2024. MaPa: Text-driven Photorealistic Material Painting for 3D Shapes. *arXiv:2404.17569*.
- Zheng, C.; Zheng, R.; Wang, R.; Zhao, S.; and Bao, H. 2021. A Compact Representation of Measured BRDFs Using Neural Processes. *ACM Trans. Graph.*, 41(2).
- Zhou, C.; Sztrajman, A.; Rainer, G.; Zhong, F.; Gokbudak, F.; Guo, Z.; Xia, W.; Mantiuk, R.; and Oztireli, C. 2024. Physically Based Neural Bidirectional Reflectance Distribution Function. *arXiv:2411.02347*.
- Zhou, C.; Zhong, F.; and Oztireli, C. 2023. CLIP-PAE: Projection-Augmentation Embedding to Extract Relevant Features for a Disentangled, Interpretable and Controllable Text-Guided Face Manipulation. In *Proceedings of ACM SIGGRAPH 2023*, 1–9.
- Zhou, Y.; Zhu, Z.; Bai, X.; Lischinski, D.; Cohen-Or, D.; and Huang, H. 2018. Non-stationary texture synthesis by adversarial expansion. *arXiv preprint arXiv:1805.04487*.